Direct-potential-fit analysis of new infrared and UV/visible $A\,^1\Sigma^+$-$X\,^1\Sigma^+$ emission spectra of AgH and AgD

Robert J. Le Roy,[a] Dominique R. T. Appadoo, Kevin Anderson, and Alireza Shayesteh
Department of Chemistry, University of Waterloo, Waterloo, Ontario N2L 3G1, Canada

Iouli E. Gordon
Department of Physics, University of Waterloo, Waterloo, Ontario N2L 3G1, Canada

Peter F. Bernath
Department of Chemistry, University of Waterloo, Waterloo, Ontario N2L 3G1, Canada, and Department of Physics, University of Waterloo, Waterloo, Ontario N2L 3G1, Canada

(Received 26 July 2005; accepted 23 August 2005; published online 21 November 2005)

New high-resolution infrared and UV/visible spectra of ^{107}AgH, ^{109}AgH, ^{107}AgD, and ^{109}AgD have been recorded with a Fourier transform spectrometer. The new line positions are combined with published microwave and older electronic $A\,^1\Sigma^+$-$X\,^1\Sigma^+$ data and used, first in a decoupled analysis of the X state alone, and then in a global multi-isotopologue analysis which yields comprehensive descriptions of both the $X\,^1\Sigma^+$ and $A\,^1\Sigma^+$ states of all four isotopologues of AgH. While the A state was long believed to be heavily perturbed, it is shown that its irregular spectrum merely reflects an unusual potential function shape. A direct fit of all data to appropriate radial Hamiltonians yields analytic potential-energy functions and Born-Oppenheimer breakdown radial functions for the ground $X\,^1\Sigma^+$ and $A\,^1\Sigma^+$ states. © *2005 American Institute of Physics*. [DOI: 10.1063/1.2064947]

I. INTRODUCTION

Metal hydrides play a central role in the organometallic chemistry of transition metals and are believed to be reaction intermediates of significant importance in various chemical reactions, particularly in catalytic processes. They are also of great astrophysical interest, due to their omnipresence in the spectra of cool stars and brown dwarfs, and they are an ideal "playground" for theoreticians to study relativistic effects on molecular properties. In addition, environmental concerns have spurred research into the use of metal hydrides for hydrogen storage for fuel cells.

The near-UV emission spectrum of AgH was first recorded by Bengtsson and Svensson in 1925,[1] but the presence of impurities prevented a thorough analysis. The first rotationally resolved UV/visible spectrum of AgH was analyzed by Hulthén and Zumstein the following year.[2] They observed the $\Delta v=1$, 0, −1, and −2 band sequences of the $A\,^1\Sigma^+$-$X\,^1\Sigma^+$ system for $v'\leqslant 3$. Five years later Bengtsson and Olsson recorded an arc emission spectrum in which they observed 27 bands corresponding to $v''(X)\leqslant 11$ and $v'(A)\leqslant 7$.[3] They only reported band origins and upper- and lower-state combination differences, but they were the first to notice the irregularities in the properties of the A state.

In 1935, Koontz measured and analyzed the 0-0 and 1-1 bands of the A-X system of AgD, with the primary objective of studying the AgH–AgD isotope shift.[4] That same year Hulthén and Knave observed and analyzed AgD transitions involving $v''(X)\leqslant 6$ and $v'(A)\leqslant 3$, but they only reported rotational constants for the observed levels.[5] It was not until 1943 that an extensive analysis of the A-X system was performed by Gerö and Schmid.[6] They recorded an arc spectrum of AgH and observed 60 bands spanning the same vibrational range covered by Bengtsson and Olsson.[3] Their primary objective was to shed light on the apparently anomalous A state, and they proposed that its irregular behavior was primarily due to homogeneous perturbation by the nearby $B\,^1\Sigma^+$ state.

Two decades later Gerö and Schmid's explanation for the anomalous behavior of the A state was disputed by Learner on the grounds that such perturbations usually result in interactions weaker than those observed in the A-X system of AgH.[7] Learner proposed instead "… that the irregularities of the spectrum, in both position and intensity, may be best explained in terms of an anomalous rotationless potential curve and its associated rotation-including potentials," and that the anomalous shape was caused by an avoided crossing of two potential curves. He combined an extrapolated inner wall with a graphical RKR-type calculation of the potential function width versus energy to construct an A-state potential-energy curve which had a substantial shelf in the interval of 2.5–4 Å. To date, his graphical curve is the only reported potential-energy function for this state that is based on empirical observations. Learner also recorded 12 bands belonging to the A-X system of AgD, and reported low-order Dunham expansion constants for both electronic states. He also found that the ratios of A-state constants for AgH and AgD were not accurately explained by the normal isotopologue mass-scaling relationships.[8] That same conclusion had been reached by Ringström in 1961 when he observed and analyzed the A-X spectrum of AgD generated in an arc.[9] In 1965, Ringström and Åslund used a King furnace to record the UV absorption of AgH and AgD.[10] They observed rovibronic transitions between five excited electronic states lying

[a]Electronic mail: leroy@uwaterloo.ca

above the first excited ($A\ ^1\Sigma^+$) state of AgH and its ground state. One of the states they observed was the $B\ ^1\Sigma^+$ state which Gerö and Schmid had proposed as being responsible for the *A*-state irregularities,[6] and they found that the *B* state showed no irregularities that could be associated with interaction with the *A* state.

In 1989, Birk and Jones generated AgH molecules in a furnace with an electrical discharge and used a diode laser spectrometer to record its first reported infrared (IR) spectrum.[11] They observed a few transitions belonging to the *P* and *R* branches of the 1-0 band and several *P* lines of both the 2-1 and 3-2 bands, and used independent fits to the two isotopologues to obtain improved ground-state Dunham constants for ^{107}AgH and ^{109}AgH. Two years later, Urban *et al.*[12] used the same experimental setup as Birk and Jones[11] to observe the first IR spectrum of AgD. Due to the intrinsic limitations imposed by diode lasers, they again only observed a few *P* and *R* lines of the fundamental and 2-1 bands, and four transitions of the 3-2 band. They combined their data with the AgH data of Birk and Jones[11] and performed a combined-isotopologue analysis which yielded accurate mass-independent and Born-Oppenheimer breakdown (BOB) mass-scaled parameters for the lower levels of the $X\ ^1\Sigma^+$ state. However, Urban *et al.*[12] were unsuccessful when they attempted to perform a direct fit of these data to a Dunham-type polynomial potential-energy function (with level energies related to the potential parameters via the usual algebraic Dunham expressions[13]), and they concluded that the "… Dunham potential does not appear to be well suited for the fitting of accurately measured transitions with high rotational quantum numbers."

The first Fourier transform (FT) infrared emission spectra of AgH and AgD were generated in a King furnace by Seto *et al.* in 1999.[14] They performed combined-isotopologue analyses of the high-resolution ground-state data and determined both conventional Dunham expansion parameters with associated BOB correction terms, and parameters defining an analytic model potential-energy function with associated adiabatic and nonadiabatic radial strength functions. The success of their potential-fit analysis showed that the problems reported by Urban *et al.*[12] were not due to the Dunham potential form itself, but rather with the fact that the earlier work had not included an atomic-mass-dependent centrifugal BOB correction function in their radial Hamiltonian. A year later Okabayashi and Tanimoto used a glow discharge to obtain the first microwave spectra of AgH and AgD and observed six rotational transitions in the ground vibrational state.[15] Combining the published IR data with their microwave data, they performed the same type of multi-isotopologue Dunham-type analysis as had Seto *et al.*,[14] and reported slightly refined Dunham and BOB parameters for the ground state of AgH.

For heavy metal hydride molecules, relativistic effects have a significant impact on *ab initio* calculations of equilibrium bond lengths, dissociation energies, dipole moments, and vibrational frequencies. Following the pioneering theoretical studies of Pyykkö and Desclaux[16] and Pyykkö[17] in the late 1970's, AgH has become a prototype molecule for the study of relativistic effects in diatomic molecules, and a series of similar studies, mainly focusing on the ground state of AgH, followed.[18–23] More recently, Witek *et al.*[24] investigated both the ground $X\ ^1\Sigma^+$ state and the anomalous first few excited states of AgH and AuH using relativistic all-electron multireference based perturbation calculations (that paper provides a thorough review of previous *ab initio* studies on these systems). Their calculated *A*-state potential-energy curve for AgH does not exhibit the broad shelf behavior proposed by Learner,[7] but it does distinctly show a qualitatively similar change in the shape of this potential at bond lengths near 3 Å. In a second study two years later, Witek *et al.*[25] focused on this anomalous behavior of the *A* state using second-order multistate multireference perturbation-theory calculations which included spin-orbit and relativistic effects. They concluded that the peculiar shape of the *A*-state potential-energy curve is due to two avoided crossings. More recently, Li *et al.*[26] reported a coupled-states treatment of the $^1\Sigma^+$ and $^3\Pi$ states of AgH. Utilizing a relativistic effective core potential for Ag, they evaluated spin-orbit interaction matrix elements between the $^1\Sigma^+$ and $^3\Pi$ states and nonadiabatic couplings among the $^1\Sigma^+$ states, and used the latter to predict nonradiative predissociative lifetimes for vibrational levels of the excited $^1\Sigma^+$ states.

The present paper reports new FT measurements of the IR spectra of the ground $X\ ^1\Sigma^+$ state and of the UV/visible $A\ ^1\Sigma^+$-$X\ ^1\Sigma^+$ electronic transitions of AgH and AgD. These new data are combined with the highly accurate microwave measurements for the ground vibrational level of the *X* state reported by Okabayashi and Tanimoto,[15] with the diode laser measurements of Birk and Jones[11] and Urban *et al.*,[12] and with the moderate-resolution UV/visible *A*-*X* data reported by Gerö and Schmid[6] to provide a comprehensive four-isotopologue, two-state data set for this system. Analysis of this global data set provides a comprehensive experimental description of the $X\ ^1\Sigma^+$ and $A\ ^1\Sigma^+$ states of ^{107}AgH and its isotopologues.

II. EXPERIMENTAL DETAILS

The UV/visible spectra of AgH and AgD and the IR spectrum of AgH were generated in a furnace-discharge emission source. Approximately 20 g of silver metal in an alumina tube was heated in a tube furnace to 1050–1350 °C. A gas stream consisting of 4 Torr of Ar and 1 Torr of H_2 or D_2 was passed through the tube, and the resulting mixture was subjected to a 3 kV/330 mA dc discharge. The emission was then focused onto the entrance aperture of a Bruker IFS 120 HR spectrometer. In the IR region, BaF_2 optics, a KBr beam splitter, and a liquid-nitrogen-cooled mercury-cadmium-telluride (MCT) detector were used. In the UV/visible region, the data were collected using quartz optics, a quartz beam splitter, and a Si photodiode detector. The IR spectrum of AgH was recorded at an unapodized resolution of 0.01 cm^{-1}, and the UV/visible spectra of AgH and AgD at 0.05 cm^{-1}.

The IR spectrum of AgD was obtained by heating a silver sample in a carbon resistance furnace (a King furnace) to temperatures exceeding 2000 °C, with a slow flow of Ar and D_2 gases passing through the system, but without using a

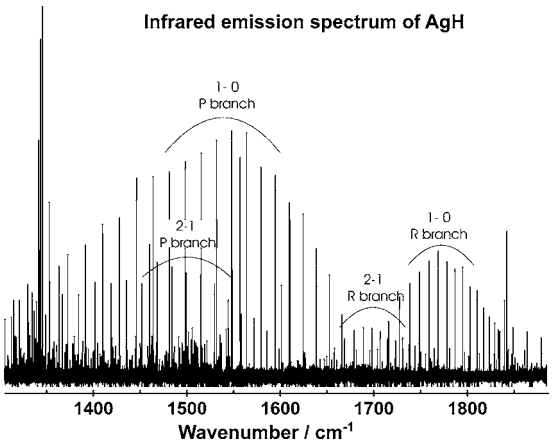

FIG. 1. A portion of our new FTIR spectrum of AgH.

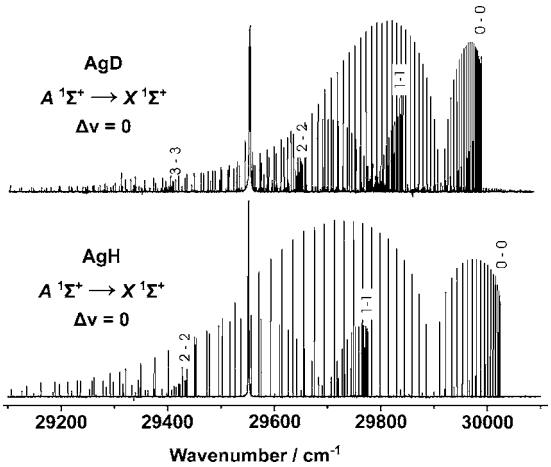

FIG. 2. Overview of our new FT spectra for the $A\ ^1\Sigma^+$-$X\ ^1\Sigma^+$ transitions of AgH and AgD.

discharge. The total pressure was held at 120 Torr, with the deuterium partial pressure being much less than that of argon. In this case we used BaF_2 optics with a KBr beam splitter and a liquid-nitrogen-cooled MCT detector. This spectrum was recorded at an unapodized resolution of 0.02 cm^{-1}.

All spectral lines positions were determined using WSPECTRA,[27] an interactive program developed by Carleer for analyzing spectral measurements. The IR spectrum of AgH was calibrated using lines of CO,[28] which was present as an impurity. The wave numbers of the lines in the UV/visible spectra were first adjusted to vacuum wave numbers using Edlén's formula[29] and then calibrated against argon lines present in our spectrum.[30] The IR spectrum of AgD was calibrated using AgH lines common to both IR spectra.

III. OVERVIEW OF THE DATA

Our previous combined-isotopologue analysis of the $X\ ^1\Sigma^+$ state of AgH was based only on our FT measurements of $\Delta v=1$ IR bands for $v''=0-3$ of ^{107}AgH, ^{109}AgH, ^{107}AgD, and ^{109}AgD.[14] The higher temperatures and longer integration times used in the present study allowed us to extend the rotational transitions for those bands to higher J and to observe the (4,3) band for AgH and and the (4,3) and (5,4) bands for AgD. For both the hydride and deuteride, all IR lines appear as doublets with relative intensities corresponding to the relative abundance of the two naturally occurring isotopes of silver, ^{107}Ag and ^{109}Ag, which differ by about 4%. The spectra appear quite simple, each band consisting of a series of doublets converging to a bandhead in the R-branch region. The signal-to-noise ratio for the most intense lines was better than 40, and typical line position uncertainties were 0.001 cm^{-1} for the (1,0) and (2,1) bands of AgH, 0.002 cm^{-1} for (3,2) and (4,3) of AgH and for (1,0)–(3,2) of AgD, 0.003 cm^{-1} for (4,3), and 0.004 cm^{-1} for (5,4) of AgD. These new data supersede those of Ref. 14. A portion of the IR spectrum of AgH recorded in this study is shown in Fig. 1.

Our new UV/visible FT A-X spectra have overlapping bands and appear slightly more complex than the IR spectra, but are still relatively simple, as both states have $^1\Sigma^+$ symmetry. The $\Delta v=0$, -1, and -2 bands for $v'=0-3$ and the $\Delta v=-1$ and -2 bands for $v'=4$ were observed for all four isotopologues, and the $(v',v'')=(5,7)$ band was observed for AgD. Except for the $\Delta v=0$ bands, for which the silver atom isotope splittings are only resolved at high rotational quantum numbers, all of these bands consist of doublets. In the UV/visible spectrum, a signal-to-noise ratio of greater than 600 was obtained for AgH. For cases in which the Ag isotope splittings were resolved, the estimated line position uncertainties were 0.005 cm^{-1}, while uncertainties of 0.01–0.05 cm^{-1} were assigned to the lower-J lines in the $\Delta v=0$ bands where those splittings were not resolved. Portions of the electronic spectra of AgH and AgD recorded in this study are shown in Fig. 2.

The diode laser IR measurements of Birk and Jones[11] and of Urban *et al.*[12] have the same accuracy as our new FT data (ca. ±0.001 cm^{-1}), although they span distinctly smaller ranges of v'' and J'', and they were included in the data set used in the present analysis. The six very precise (uncertainties of $\sim 10^{-6}$ cm^{-1}) microwave transitions for ground-state $v''=0$ isotopologues observed by Okabayashi *et al.*[15] were also used in our analysis. Their very high precision and the fact that transitions were obtained for all four isotopic species make these data particularly important with regard to the determination of the equilibrium bond length and rotational BOB effects.

Figure 3 compares the domains of our new FT results for the A-X system with those of Gerö and Schmid,[6] for which the entries are denoted "g" or "G" depending on whether (G) or not (g) they were used in our final analysis, and of Ringström[9] and Ringström and Åslund[10] (entries denoted "r"). While the precision and accuracy of the earlier measurements are much lower than those of our FT results, the hydride data of Gerö and Schmid[6] extend to $v'(A)=7$ and $v''(X)=11$, well beyond the range of our new FT data. The seven bands they obtained for which $v'\geqslant 5$ and/or $v''\geqslant 8$ (denoted G in Fig. 3) were therefore included in the data set used in the present analysis. Fits to individual bands confirmed that the Gerö-Schmid data had precision of order of ±0.1 cm^{-1}. However, for the four Gerö-Schmid bands in common with the FT results, (0,0), (1,2), (2,3), and (3,5), the fitted band origins differed from those obtained from our FT

v′\v″	0	1	2	3	4	5	6	7	8	9	10	11
0	⊗ g r	⊗ r	⊗		g							
1	r	⊗ r	⊗ g r	⊗			g					
2		r	⊗ r	⊗ g r	⊗ r		g					
3		g	r	⊗ r	⊗ r	⊗ g r						
4				g		⊗ r	⊗ r			G		
5								x	G		G	
6				G							G	
7										G		G

FIG. 3. Summary of spectroscopic information for the *X* and *A* states of AgH and AgD. Our new FT data are denoted "○ for" the hydride and "×" for the deuteride; "m" identifies the microwave data of Ref. 15, "r" the early electronic data of Ringström (Ref. 9) and Ringström and Åslund (Ref. 10), "d" the hydride and deuteride diode laser IR data of Refs. 11 and 12, and "g" and "G" the electronic AgH data of Gerö and Schmid,[6] where "G" identifies the subset of the latter used in this analysis.

data by amount ranging from −0.12 to +0.15 cm^{-1}. The uncertainties assigned to the Gerö-Schmid data used in the present analysis were therefore 0.15 cm^{-1}; however, the absolute uncertainties associated with the energies of AgH vibrational levels with $v' \geqslant 5$ and $v'' \geqslant 8$ may be somewhat larger than that.

A complete listing of data used in this study may be obtained from the Journal's online www archive[31] or from the authors.

IV. ANALYSIS METHODOLOGY

A. "Parameter-fit" models

In an empirical analysis of spectroscopic data, the vibration-rotation level energies of a $^1\Sigma^+$ electronic state may be treated at three general levels of sophistication.

(i) In the most basic approach, the parameters in the fit are simply the term values of all the individual vibration-rotation levels $T_{v,J}^{(\alpha)}$, where α identifies the particular isotopologue. This is appropriate if the state in question is heavily perturbed and one wishes to obtain level energies unbiased by the assumptions of a particular model, and/or to ensure that parameters being determined for another electronic state are not biased by irregular behavior of the state in question. However, it requires a relatively large number of fitting parameters, and it provides no physical or mathematical model for the quantum number dependence of the molecular properties.

(ii) If the rotational term values are generally well behaved, the rotational energies for each vibrational level of a given isotopologue "α" may be represented by band constants

$$E_{v,J}^{(\alpha)} = \sum_{m=0} K_m^{(\alpha)}[J(J+1)]^m = G_v^{(\alpha)} + B_v^{(\alpha)}[J(J+1)] - D_v^{(\alpha)}[J(J+1)]^2 + H_v^{(\alpha)}[J(J+1)]^3 + \ldots . \quad (1)$$

This provides a more compact description of the level energies, although it still requires one to determine and tabulate independent values of all appropriate band constants for each observed vibrational level of each molecular isotopologue. It also leaves us with a limited overall physical model, and a very limited ability to extrapolate to predict unobserved data.

(iii) If the band constants for vibration and/or rotation are smooth functions of v, they may in turn be represented by analytic functions such as the familiar Dunham double power series expansion, with isotope effects being taken into account both by the conventional semiclassical reduced-mass quantum number scaling and by additional correction terms. Using the notation of Ref. 32, the vibrational and isotope dependence of each type of band constant is described by the expression

$$K_m^{(\alpha)}(v) = \sum_{l=0}^{l_{\max}(m)} Y_{l,m}^{(\alpha)}\left(v+\frac{1}{2}\right)^l = \sum_{l=0}^{l_{\max}(m)} \left(\frac{\mu_1}{\mu_\alpha}\right)^{m+l/2}\left\{Y_{l,m}^{(1)} + \frac{\Delta M_A^{(\alpha)}}{M_A^{(\alpha)}}\delta_{l,m}^A + \frac{\Delta M_B^{(\alpha)}}{M_B^{(\alpha)}}\delta_{l,m}^B\right\}\left(v+\frac{1}{2}\right)^l, \quad (2)$$

in which μ_α is the normal reduced mass of isotopologue α formed from atoms A and B with masses $M_A^{(\alpha)}$ and $M_B^{(\alpha)}$, respectively, $\Delta M_{A/B}^{(\alpha)} = M_{A/B}^{(\alpha)} - M_{A/B}^{(1)}$, and $\alpha = 1$ identifies a chosen "reference" isotopologue. This type of representation is particularly compact, since a full set of Dunham-type parameters $\{Y_{l,m}^{(1)}\}$ is required only for the reference species $\alpha = 1$, while high-order semiclassical and BOB effects usually only require a relatively modest number of BOB parameters $\delta_{l,m}^{A/B}$ to be introduced. Moreover, the resulting analytic expressions for G_v and B_v may be used to calculate an RKR potential-energy curve for this state. Fits of this type may also be performed using near-dissociation expansions.[33–37] (NDEs) or mixed Dunham/NDE expressions[37–39] to represent the $K_m^{(\alpha)}(v)$ functions.[37]

The present analysis was performed using program DPARFIT which can use different choices (i)–(iii) for the models describing different electronic states and/or for different types of contributions (i.e., vibrational versus rotational versus centrifugal distortion) to the level energies for a given electronic state, in a single analysis.[37] Throughout the following, the quality of fit associated with a fit of N data $y_{\rm obs}(i)$ with uncertainties $u(i)$ to a given model is represented by the dimensionless root-mean-square deviation,

$$\overline{dd} \equiv \left\{\frac{1}{N}\sum_{i=1}^{N}\left[\frac{y_{\rm calc}(i) - y_{\rm obs}(i)}{u(i)}\right]^2\right\}^{1/2}, \quad (3)$$

in which $y_{\rm calc}(i)$ is the value of datum i calculated from that model. When comparing the ability of different types of models to represent our data, this quantity is more useful than the familiar dimensionless standard deviation for a fit to an M-parameter model, $\bar{\sigma}_f = \overline{dd}\sqrt{N/(N-M)}$, since the differ-

ent models considered here have substantially different numbers of free parameters.

B. Direct-potential-fit (DPF) treatment

If a full Dunham-type treatment of approach (iii) is feasible for a given system, it usually means that the relevant electronic states are "mechanical," in that their spectra may be fully explained in terms of the properties of a potential-energy function and associated atomic-mass-dependent BOB radial strength functions. In the notation of Ref. 32, this means that the observed vibration-rotation level energies of each isotopologue (α) are accurately described as eigenvalues of the radial Schrödinger equation,

$$\left\{-\frac{\hbar^2}{2\mu_\alpha}\frac{d^2}{dr^2}+[V_{\rm ad}^{(1)}(r)+\Delta V_{\rm ad}^{(\alpha)}(r)] + \frac{\hbar^2 J(J+1)}{2\mu_\alpha r^2}[1+g^{(\alpha)}(r)]\right\}\psi_{v,J}(r)=E_{v,J}\psi_{v,J}(r), \quad (4)$$

in which $V_{\rm ad}^{(1)}(r)$ is the total internuclear potential for the selected reference isotopologue (labeled $\alpha=1$), $\Delta V_{\rm ad}^{(\alpha)}(r)$ is the *difference* between the effective adiabatic potentials for isotopologue α and for the reference species ($\alpha=1$), and $g^{(\alpha)}(r)$ is the nonadiabatic centrifugal potential correction function for isotopologue α. Both $\Delta V_{\rm ad}^{(\alpha)}(r)$ and $g^{(\alpha)}(r)$ are written as a sum of two terms, one for each component atom, whose magnitudes are inversely proportional to the mass of the particular atomic isotope,[32,40–43]

$$\Delta V_{\rm ad}^{(\alpha)}(r)=\frac{\Delta M_A^{(\alpha)}}{M_A^{(\alpha)}}\tilde{S}_{\rm ad}^{A}(r)+\frac{\Delta M_B^{(\alpha)}}{M_B^{(\alpha)}}\tilde{S}_{\rm ad}^{B}(r), \quad (5)$$

$$g^{(\alpha)}(r)=\frac{M_A^{(1)}}{M_A^{(\alpha)}}\tilde{R}_{\rm na}^{A}(r)+\frac{M_B^{(1)}}{M_B^{(\alpha)}}\tilde{R}_{\rm na}^{B}(r), \quad (6)$$

where the empirical expressions used to define $\tilde{S}_{\rm ad}^{A/B}(r)$ and $\tilde{R}_{\rm na}^{A/B}(r)$ are presented below. A straightforward extension of this approach to take account of the e/f Λ-doubling splitting which arises for states with $\Lambda\neq 0$ was described in Ref. 44.

In a DPF analysis, a direct fit of experimental transition energies to eigenvalue differences calculated from the radial Hamiltonian is used to determine parameters defining the potential-energy and the related BOB radial functions. This is a fully quantum-mechanical approach which tends to yield a particularly compact set of empirical parameters, and the resulting potential-energy and radial correction functions may be used to predict other system properties. The DPF analyses reported herein were performed using program DPOTFIT.[45]

For both the X and A states, the model used for the reference-isotopologue potential-energy function $V_{\rm ad}^{(1)}(r)$ is what we call an "extended Morse oscillator," or EMO_p potential form. It is a straightforward extension of the familiar Morse potential in which the exponent coefficient is allowed to vary with distance:

$$V_{\mathrm{EMO}_p}(r)=\mathfrak{D}_e[1-e^{-\beta(y_p)\cdot(r-r_e)}]^2, \quad (7)$$

where $\mathfrak{D}_e$ is the well depth, r_e the equilibrium distance, and the exponent coefficient in Eq. (7) is expressed as a simple power series expansion,

$$\beta_{\mathrm{EMO}_p}=\sum_{i=0}^{N}\beta_i y_p^i, \quad (8)$$

in which the expansion variable is a version of a generalized expansion variable introduced by Šurkus *et al.*:[46]

$$y_p=y_p(r)=\frac{r^p-r_e^p}{r^p+r_e^p}. \quad (9)$$

Huang and co-workers have shown that defining the exponent coefficient as an expansion in the variable $y_p(r)$, for some appropriate small integer value of $p>1$ (say, $p=2$–4), greatly reduces the probability that the resulting potential function will exhibit nonphysical behavior (e.g., turn over) at distances outside the radial interval to which the data are sensitive.[44,47,48] For the same reason, they found that it is also sometimes desirable to allow the polynomial in Eq. (8) to have a lower order in the short-range repulsive wall region than in the attractive outer well region. Thus, a particular type of EMO potential is identified by the label $\mathrm{EMO}_p(N_S,N_L)$, where the polynomial order in Eq. (8) is $N=N_S$ when $r<r_e$ and $N=N_L$ when $r\geqslant r_e$. One drawback of having $N_S\neq N_L$ is that derivatives of the potential of order $\min\{N_S,N_L\}+2$ will not be continuous at the one point $r=r_e$; however, since $\min\{N_S,N_L\}$ is typically $\geqslant 4$, this is not a serious shortcoming.

Following the discussion of Refs. 48 and 44 the radial strength functions for the potential-energy and centrifugal BOB corrections are written in the forms[42]

$$\tilde{S}_{\rm ad}^{A}(r)=[1-y_p(r)]\sum_{i=0}u_i^A[y_p(r)]^i+u_\infty^A y_p(r), \quad (10)$$

$$\tilde{R}_{\rm na}^{A}(r)=[1-y_p(r)]\sum_{i=0}t_i^A[y_p(r)]^i+t_\infty^A y_p(r), \quad (11)$$

for atom $A=$Ag or H. Use of this form allows the appropriate asymptotic behavior and differences in well depths for different isotopologues to be treated explicitly.[48] For the ground state, the value of $u_0^{\rm H}$ defines the difference between the well depths for the hydrogenic isotopologues, $\delta\mathfrak{D}_e(X)=(\Delta M_{\rm H}^{(\alpha)}/M_{\rm H}^{(\alpha)})u_0^{\rm H}$, while $u_\infty^{\rm H}=u_\infty^{\rm Ag}=0$ by definition.[48] For the A state, the difference $u_0^{\rm H}(A)-u_0^{\rm H}(X)$ determined the electronic isotope shift and $u_\infty^{\rm H}(A)-u_0^{\rm H}(A)$ the isotopic differences in the well depths.

Finally, we note that the integer p used to define the radial variables in Eqs. (10) and (11) need not be the same as that used for the potential function itself, but it is usually convenient to do so. FORTRAN code for generating these potential-energy and BOB radial functions may be found in subroutine POTGEN which is part of the freely available radial Schrödinger solver package LEVEL.[49]

TABLE I. Results of fits to the the global data set performed while representing the $A\,^1\Sigma^+$ state with an independent term value for each observed level.

		No. of parameters			
X-state model	$\mathcal{D}_e$	X state	A state	Total	$\overline{dd}$
All band constants	···	156	911	1067	0.889
All Dunham	···	30	911	941	0.911
$EMO_2(7,7)$ potential	19 145(±7.3)	15	911	926	0.942
$EMO_3(7,7)$ potential	19 235(±3.5)	**15**	**911**	**926**	**0.927**
$EMO_4(7,7)$ potential	19 534(±3.8)	15	911	926	1.732
$EMO_2(8,8)$ potential	19 274(±25.)	16	911	927	0.921
$EMO_3(8,8)$ potential	19 215(±6.2)	16	911	927	0.920
$EMO_4(8,8)$ potential	19 434(±3.6)	16	911	927	1.149

V. RESULTS

A. Treatment of the $X\,^1\Sigma^+$ state

It is well known that the $A\,^1\Sigma^+$ state of AgH has an unusual or irregular behavior[3,6,7] and that the $X\,^1\Sigma^+$ state is "well behaved."[12,14] The initial stage of our analysis therefore set out to determine the best possible models for the latter in a manner which was unbiased by any assumptions about the behavior of the former. To this end, in these initial fits to the four-isotopologue data set, the A state was represented by an independent term value $T_{v,J}^{(\alpha)}$ for each distinct observed vibration-rotation level of each isotopologue [model (i) of Sec. IV A]. The large number of such term values means that there are a fairly large number of fitting parameters, but this presents no practical difficulties.[37,45] This is not, in principle, an optimum treatment because the uncoupling from a model for the A state means that only the spacings between levels with a common A-state level are taken into account, and this reduces the quality of information which might otherwise be obtainable about the X state. However, it allows us to determine appropriate ways of describing the X state, and if the A-state levels were very heavily perturbed it would be the best approach possible without invoking an explicit deperturbation analysis.

Table I summarizes properties of seven combined-isotopologue fits to the global data set, all performed with the levels of the A state being represented by term values. In what we chose as our optimum "parameter-fit" treatment of the $X\,^1\Sigma^+$ state, its level energies were represented by 26 Dunham $Y_{l,m}$ parameters and four BOB $\delta_{l,m}^{\mathrm{H}}$ parameters, while the $A\,^1\Sigma^+$ state was represented by 911 independent term values. This recommended X-state model is defined by Dunham-expansion orders $l_{\max}(m)=6$, 6, 5, 1, and 4 for $m=0$–4, respectively, and $l_{\max}(m)=2$ and 1 for the H-atom BOB $\delta_{l,m}^{\mathrm{H}}$ terms for $m=0$ and 1, respectively. The associated overall quality of fit $\overline{dd}=0.911$ indicates that this model accounts for all observables (on average) within their estimated uncertainties. This treatment neglects 75 observed transitions involving A-state levels which are connected to only a single X-state level, as they provide no information about the $X\,^1\Sigma^+$ state.

The results for direct potential fits using a selection of models for the $X\,^1\Sigma^+$ state are listed in the last six rows of Table I. Each of these fits also determined a potential-energy BOB function $\tilde{S}_{\mathrm{ad}}^{\mathrm{H}}(r)$ defined by the three nonzero parameters u_1^{H} to u_3^{H}, and a centrifugal BOB function $\tilde{R}_{\mathrm{na}}^{\mathrm{H}}$ defined by the two nonzero parameters t_1^{H} and t_2^{H}. Following the conventions of Ref. 48, $u_\infty^{\mathrm{Ag/H}}=0$ for electronic states formed from ground-state atoms, $t_0^{\mathrm{Ag/H}}=0$, and $t_\infty^{\mathrm{Ag/H}}=0$ since AgH is a

TABLE II. Results of fits to the global data set performed on combining various models for the $X\,^1\Sigma^+$ and $A\,^1\Sigma^+$ states of AgH.

Model for this state			No. of parameters			
X state	A state	$\mathcal{D}e(X)$ cm^{-1}	X state	A state	Total	$\overline{dd}$
All Dunham	All term values $T_{v,J}^{(\alpha)}$	···	30	911	941	0.911
All Dunham	All band constants	···	30	164	194	1.135
All Dunham	Dunham G_v plus rotational band constants	···	30	151	181	1.139
All Dunham	Dunham G_v and B_v plus CDC band constants	···	30	135	165	1.151
All Dunham	All Dunham: 63 $Y_{l,m}$ plus 28 BOB parameters	···	30	91	121	1.136
$EMO_3(7,7)$	$EMO_3(5,10)$:[a] 13 potential and 12 BOB function parameters	19 233(±1.8)	15	25	40	1.407
$EMO_3(7,7)$	$EMO_4(5,10)$: 13 potential and 12 BOB function parameters	19 247(±1.8)	15	25	40	1.133
$EMO_3(7,7)$	$EMO_4(6,10)$: 13 potential and 12 BOB function parameters	19 250(±2.0)	15	25	40	1.274

[a]This potential turns over at short range.

TABLE III. Recommended Dunham-type parameter set describing the $X\,^1\Sigma^+$ state of AgH, all in units cm^{-1}. The numbers in parentheses represent 95% confidence limit uncertainties in the last digits shown.

Constant	^{107}AgH	^{109}AgH	^{107}AgD	^{109}AgD
$Y_{1,0}$	1759.9586 (40)	1759.807 692	1250.943 508	1250.731 12
$Y_{2,0}$	−34.180 47(440)	−34.174 608 6	−17.267 5532	−17.261 6902
$10^3\times Y_{3,0}$	66.4 (21)	66.382 92	23.832 53	23.820 39
$10^3\times Y_{4,0}$	−7.871(490)	−7.8683	−2.007 702	−2.006 339
$10^6\times Y_{5,0}$	−140.(53)	−139.94	−25.3784	−25.3569
$10^6\times Y_{6,0}$	−17.1(22)	−17.0912	−2.202 93	−2.200 68
$Y_{0,1}$	6.449 965 9 (72)	6.448 859 84	3.257 853 8	3.256 747 64
$Y_{1,1}$	−0.201 928 3(220)	−0.201 876 361	−0.072 499 257	−0.072 462 336
$10^6\times Y_{2,1}$	467.(21)	466.84	119.1204	119.0396
$10^6\times Y_{3,1}$	−16.(8)	−15.9931	−2.900 39	−2.897 93
$10^6\times Y_{4,1}$	−14.923(1600)	−14.915 32	−1.922 473	−1.920 516
$10^6\times Y_{5,1}$	1.013 (160)	1.012 392	0.092 743	0.092 632 8
$10^9\times Y_{6,1}$	−52.(6)	−51.9643	−3.383 31	−3.378 72
$10^6\times Y_{0,2}$	−346.42(3)	−346.3012	−88.363 393	−88.303 398
$10^6\times Y_{1,2}$	4.214 (38)	4.212 19	0.763 891	0.763 243
$10^9\times Y_{2,2}$	−80.(30)	−79.959	−10.3061	−10.2956
$10^9\times Y_{3,2}$	−98.5(100)	−98.4409	−9.017 95	−9.007 24
$10^9\times Y_{4,2}$	11.9 (15)	11.891 84	0.774 258	0.773 207
$10^{12}\times Y_{5,2}$	−828.(77)	−827.361	−38.2857	−38.2272
$10^9\times Y_{0,3}$	10.75 (6)	10.744 47	1.384 881	1.383 471
$10^9\times Y_{1,3}$	−0.73(3)	−0.729 56	−0.066 834	−0.066 754
$10^{15}\times Y_{0,4}$	−640.(33)	−639.56	−41.641	−41.584
$10^{15}\times Y_{1,4}$	180.(30)	179.86	8.323	8.3103
$10^{15}\times Y_{2,4}$	−131.3(160)	−131.187	−4.314 58	−4.307 26
$10^{15}\times Y_{3,4}$	31.(4)	30.9708	0.723 94	0.722 589
$10^{15}\times Y_{4,4}$	−3.28(32)	−3.276 63	−0.054 435 5	−0.054 324 7
$\delta^{H}_{1,0}$	0.5507 (15)			
$\delta^{H}_{2,0}$	−0.0186(4)			
$10^3\times\delta^{H}_{0,1}$	1.173 (4)			
$10^3\times\delta^{H}_{1,1}$	−0.125(4)			

neutral molecule. As mentioned above, for the ground state, $u_0^{Ag/H}$ determines the differences between the well depths for the different isotopologues. However, such differences are normally not expected to be more than a few cm^{-1}, even for hydrides, and since the highest observed vibrational level lies more than 3500 cm^{-1} below the dissociation limit, we cannot expect such differences to be discerned in the present analysis, so our fits fixed $u_0^{Ag}=u_0^{H}=0$. Of course, for an excited electronic state the values of $u_0^{Ag/H}$ (or more correctly, the differences between these quantities for the ground and excited states) determine the electronic isotope shifts for the different isotopologues (see Sec. V B).

Unlike Dunham expansions, most DPF fits naturally treat the well depth $\mathfrak{D}_e$ as one of the fitting parameters, although it can be held fixed if an accurate value is known from some other source. The contrast between the differences among the various fitted values of $\mathfrak{D}_e$ and the (correlated 95% confidence limit) uncertainties yielded by the fits (see Table I) illustrates the well-known fact that model dependence is often a much larger source of uncertainty than the correlated parameter uncertainty determined within a particular model.[35] These fitted values are fairly similar to the 19 260 cm^{-1} listed by Huber and Herzberg.[50] However, they differ substantially both from the "third-law" thermochemical value of 18 534(±700) cm^{-1} [or $\mathfrak{D}_0$ =50.5(±2.) kcal/mol] recommend by Kant and Moon,[51] and from their "second-law" value of 19 863(±350) cm^{-1}.[51] These thermodynamic values are outside the range which seem acceptable to the spectroscopic data. Thus, within an estimated real physical uncertainty of ±200 cm^{-1} we believe that the present DPF analysis will yield as good a dissociation energy as may be obtained at this time. However, for reasons stated above, we will leave our final recommended value to be specified by the full two-state analysis reported below.

In summary, the results presented in Table I show that an excellent direct potential fit to the *X*-state data alone may be obtained using a number of different potential function models. The poorer quality of fit obtained when the radial variable $y_p(r)$ was defined with $p=4$ illustrates the fact that while setting $p>1$ helps make the potential function more stable in the extrapolation region, for too high values the quality of fit always eventually degrades.[44,47,48] Because it requires fewer fitted parameters than the other "good" cases, and because its fitted $\mathfrak{D}_e$ value was in the center of the range, we chose an $EMO_3(7,7)$ potential and the associated ($p=3$) BOB functions (bold font case in row 4 of Table I) to represent the $X\,^1\Sigma^+$ state in the two-state fits described below. While the values of $\overline{dd}$ for the direct potential fits are slightly larger than that for the all-Dunham fit, this is to be expected be-

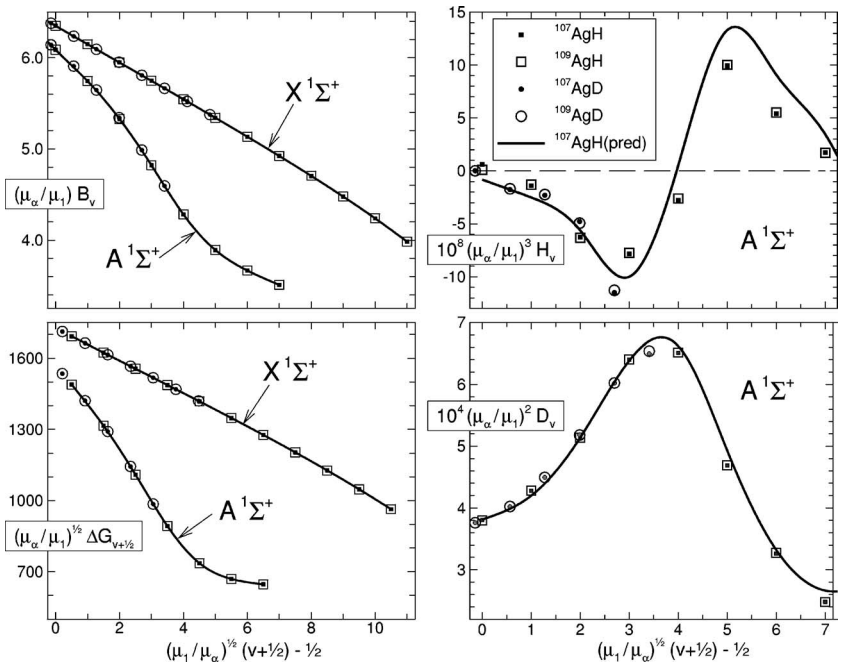

FIG. 4. Mass-scaled band constants for the four isotopologues of AgH: the solid points are those including ^{107}Ag and open points for ^{109}Ag; the square points are for the hydrides and round points for deuterides.

cause our empirical Dunham-type parameter fit did not require physical consistency between the G_v and B_v values and the centrifugal distortion constants (CDCs), while such "mechanical consistency" is implicitly imposed by a DPF analysis.

B. Treatment of the $A\,^1\Sigma^+$ state

Irregular patterns in the spectra of the $A\,^1\Sigma^+$ state of AgH had led to suggestions that it was heavily perturbed,[6] and no previous analysis has yielded a quantitative comprehensive description of this state. The present treatment therefore began with an examination of the degree to which it could be accurately described by a parameter-fit analysis. To this end, a series of fits was performed in which the $X\,^1\Sigma^+$ state was represented by the optimal Dunham-type model described above while increasingly sophisticated models were used for the A state. The second row of Table II shows that when the term-value treatment of Table I (listed again as the first row of Table II) was replaced by the band constant representation of Eq. (1), the number of independent parameters required to describe the A state is substantially reduced and a good quality of fit is obtained. The fact that the use of band constants rather than term values causes the value of $\overline{dd}$ to increase by 25% is to be expected and carries no physical significance, since the term-value representation assumes no physical model for levels of the A state, and takes no account of experimental uncertainties in the A-state level positions. Thus, the resulting value of $\overline{dd}=1.135$ still represents a completely satisfactory representation of the data, within its estimated uncertainties.

The next question to address is whether the vibrational energies and rotational constants are smooth functions of the vibrational quantum number, and whether the conventional generalized Dunham-type combined-isotopologue expressions of Eq. (2) would be valid for this case. The third and fourth rows of Table II show that good fits are also obtained if G_v, or both G_v and B_v are represented by the Dunham-type polynomials of Eq. (2), while row 5 shows that a full empirical Dunham-type treatment also gives a completely satisfactory description of the data. Progression through these five cases also leads to an order-of-magnitude reduction in the number of empirical parameters required to describe the A state (from 911 to 91) with no physically significant cost in the quality of fit.

The parameters for the X state obtained from the full "all Dunham" analysis associated with the fifth row of Table II are listed in Table III. The first column lists the reference-isotopologue parameters actually determined by the fit while the last three columns list the derived [from Eq. (2)] $Y_{l,m}^{(\alpha)}$ values describing the "minor isotopologues." The numbers of significant digits shown were determined by the automatic "sequential rounding and refitting" procedure discussed in Ref. 52 [as implemented in our general least-squares subroutine NLLSSRR (Ref. 53)], and suffice to reproduce the data with no significant loss of precision.

The analogous table of Dunham-type parameters for the A state is more than three times as long as that for the X state, so it is only presented in the journal's online data archive.[31] Although the energy and vibrational level ranges are distinctly smaller than for the X state, the unusual shape of the A state requires higher-order polynomials to be used for all band constants, and the number of BOB parameters required is a much larger fraction of the total number of parameters required to represent the level energies (28 out of 91 versus 4 out of 30 for the X state).

In principle, almost any function may be fitted by polynomials having a sufficiently large number of terms, so the mere fact that an adequate Dunham-type fit can be obtained does not in itself confirm that the $A\,^1\Sigma^+$ state of AgH is "mechanical," i.e., that its properties may be accurately described by a potential-energy curve and BOB radial functions. To examine this point further, Fig. 4 shows the leading band constants yielded by the full band-constant fit of row 2

of Table II, for all observed vibrational levels of all four isotopologues (points), plotted in the manner suggested by the conventional first-order semiclassical mass scaling of Eq. (2). It is clearly evident that to within realistic uncertainties, all of the fitted values for the different isotopologues are associated with some internally consistent smooth functional behavior. The distinct "hooks" in the plots of G_v and B_v for the A state (left side of Fig. 4) contrast sharply with the "regular" behavior of those properties for the X state. Together with the unusual oscillatory behavior of the D_v and H_v constants, this clearly illustrates the anomalous nature of the this state. Plots of this type also illustrate why it is meaningful to use Dunham polynomials of order equal to or higher than the number of observed vibrational levels of any one isotopologue since the values for the other isotopologues provide independent additional points on the same plot.

While the internal consistency among the results for the different isotopologues shown in Fig. 4 provides fairly convincing evidence of the mechanical nature of the A state, our empirical Dunham fit did not require physical consistency between the different types of band constants. However, within a semiclassical analysis, knowledge of G_v and B_v allows the potential-energy curve to be determined by the RKR method,[54,55] and distortion constants are merely derived properties of that potential, and not independent parameters. As a final test, therefore, the G_v and B_v polynomials yielded by our Dunham analysis were used to generate a RKR potential curve for the reference isotopologue ^{107}AgH,[55] and that potential function was used in the standard quantum-mechanical procedure for calculating centrifugal distortion constants from a known potential function.[49,56] The resulting values of D_v and H_v define the solid curves on the right-hand side of Fig. 4. The suprisingly good semiquantitative agreement with the empirical band-constant values (points) clearly confirms that the $A\ ^1\Sigma^+$ state of AgH is indeed mechanical. At the same time, the oscillatory behavior of these distortion constants and the associated hooks in the plots of G_v and B_v attest to the validity of Learner's assertion about the anomalous nature of that potential function. However, the still rather large number of fitting parameters (91) and the fact that the BOB "correction" function parameters $\delta^{\mathrm{H}}_{l,m}$ for the higher-order distortion constants[31] have the same magnitude as the corresponding $Y_{l,m}$ coefficients[31] indicate that this all-Dunham treatment does not provide an optimal compact physical description of this state. For the user's convenience, an ASCII listing of the complete parameter set of Table III and of the analogous Dunham-type parameter listing for the A state, together with a listing of the associated band constants for all observed levels of all four isotopologues, may be obtained from the journal's online data archive.[31]

In view of the above, the final stage of the present analysis consisted of simultaneous two-state direct potential fits to all of the multiple-isotopologue data. In any DPF analysis it is necessary to obtain realistic initial trial potential function parameters in order to initiate a stable fitting sequence, and doing so is particularly challenging for a potential function with an unusual shape. However, fits of Eq. (7) to RKR turning points did provide adequate starting points. Further problems arise from the fact that the anomalous shape of the A-state potential requires a relatively large number of terms in the exponent expansion of Eq. (8), and this in turn increases the propensity for the potential function to turn over in the long- and/or short-range "extrapolation regions," outside the interval directly probed by the experimental data. These considerations lead to a preference for potential functions based on relatively large values of the integer p defining the radial expansion variable $y_p(r)$, and the use of different expansion powers in the short-range (where $N=N_S$) and long-range (where $N=N_L$) regions.[44,47,48]

The last three rows of Table II summarize results obtained using three different models for the A-state potential, all based on a maximum exponent order of $N_L=10$, but with different values of p and/or N_S. The quality of fit yielded by the first of these models, an $\mathrm{EMO}_3(5,10)$ potential, is slightly less than optimal; while that could be improved by increasing the exponent polynomial "outer order" beyond $N_L=10$, all A-state models for which $p\leqslant 3$ yielded potentials which turned over at short range, outside the data region. The fact that the $\overline{dd}$ values associated with the $\mathrm{EMO}_4(6,10)$ fit is slightly higher than that for the $\mathrm{EMO}_4(5,10)$ case reflects the fact that for the given fixed maximum exponent polynomial order of $N_L=10$, the potential form requires additional flex-

TABLE IV. Parameters defining the recommended potential-energy and BOB radial functions for the $X\ ^1\Sigma^+$ and $A\ ^1\Sigma^+$ states of AgH; numbers in parentheses are 95% confidence limit uncertainties in the last digits shown. The analysis assumes that the A-state asymptote lies 29 552.05 cm^{-1} above that of the X state (Ref. 57). The value of $\mathfrak{D}_e(X)$ was fixed at 19 250 cm^{-1} in the final fit.

Parameter	X state	A state
Form	$\mathrm{EMO}_3(7,7)$	$\mathrm{EMO}_4(5,10)$
T_e(cm^{-1})	0.0	29 971.4049 (49)
$\mathfrak{D}_e$(cm^{-1})	19 250 [±200[a]]	18 830.6461 [±200[a]]
r_e(Å)	1.617 916 2 (1)	1.644 795 (1)
β_0	1.543 580 95 (7200)	1.451 670 7 (700)
β_1	0.037 386 (70)	−0.250 919(200)
β_2	0.166 424 (55)	−0.269 068(1200)
β_3	0.098 03 (33)	−0.405 74(300)
β_4	0.170 89 (110)	−1.114 35(2200)
β_5	0.0602 (19)	−1.5645(380)
β_6	0.140 (6)	25.9742 (5700)
β_7	0.224 (6)	−96.593(1800)
β_8	⋯	162.66 (260)
β_9	⋯	−127.12(180)
β_{10}	⋯	38.1 (5)
u_0^{Ag}(cm^{-1})	0.0	−0.62(3)
u_0^{H}(cm^{-1})	0.0	−20.991(9)
u_1^{H}(cm^{-1})	11.75 (3)	118.55 (15)
u_2^{H}(cm^{-1})	17.56 (10)	−151.65(86)
u_3^{H}(cm^{-1})	−12.7(6)	132.6 (79)
u_4^{H}(cm^{-1})	⋯	−594.(16)
u_5^{H}(cm^{-1})	⋯	−536.(60)
u_6^{H}(cm^{-1})	⋯	3150.(160)
u_7^{H}(cm^{-1})	⋯	−2140.(120)
q_1^{H}	0.000 15 (1)	0.000 289 (27)
q_2^{H}	0.000 93 (5)	0.002 98 (15)
q_3^{H}	⋯	0.0080 (1)

[a]Uncertainty estimate based largely on model dependence; see text.

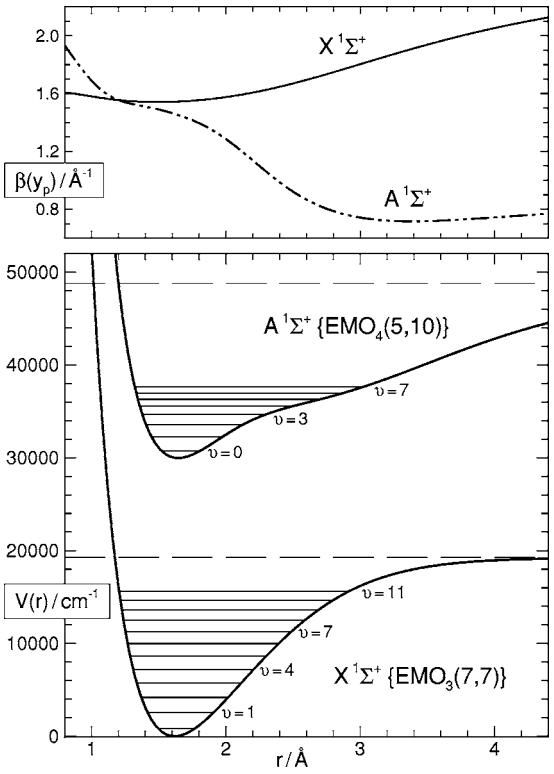

FIG. 5. *Lower*: potential-energy functions determined for the $X\,^1\Sigma^+$ and $A\,^1\Sigma^+$ states of AgH, with energy levels indicating the experimental domain; *Upper*: distance-dependent exponent coefficient functions for these EMO$_p$ potentials.

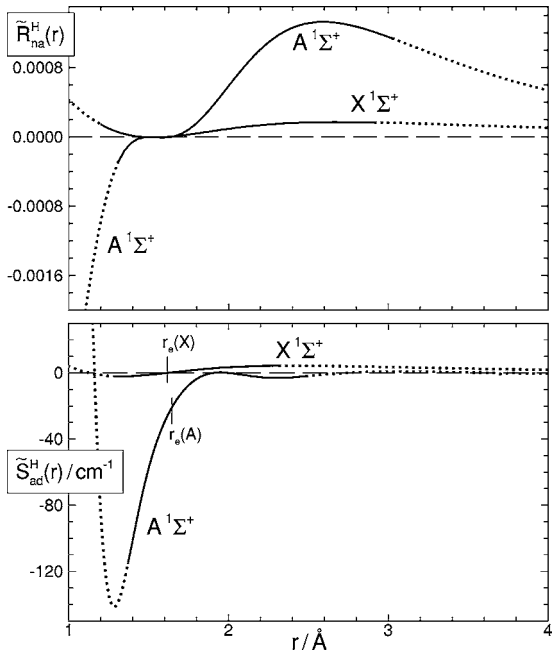

FIG. 6. *Lower*: potential-energy radial BOB functions determined for the $X\,^1\Sigma^+$ and $A\,^1\Sigma^+$ states of AgH; *Upper*: centrifugal BOB radial functions determined for the $X\,^1\Sigma^+$ and $A\,^1\Sigma^+$ states of AgH. In both cases, the curves are drawn as dotted in the extrapolation regions and solid on the domain of the data which determine that property.

ibility in the region $r \geqslant r_e$. Thus, the EMO$_4$(5,10) potential is our recommended model for the $A\,^1\Sigma^+$ state potential-energy function. However, since our estimate of the real physical uncertainty in the ground-state dissociation energy is ± 200 cm^{-1}, our final parameter-rounding fit was performed using a fixed rounded value of $\mathfrak{D}_e(X) = 19\,250$ cm^{-1} in place of the value (19 247) seen in Table II.

The *X*- and *A*-state potential-energy and BOB function parameters defining our final recommended models for the $X\,^1\Sigma^+$ and $A\,^1\Sigma^+$ states of AgH and AgD are listed in Table IV. Since the reference isotopologue in our analysis was ^{107}AgH, the effective adiabatic potential curves for the other isotopologues may be generated by adding the $\Delta V^{(\alpha)}_{\rm ad}(r)$ function obtained on substituting appropriate values of $M^{(\alpha)}_{\rm Ag}$ and $M^{(\alpha)}_{\rm H}$ in Eq. (5). Our recommended rotationless potentials for ^{107}AgH are shown in Fig. 5; the hydride level energies and turning points shown there indicate the domain of the experimental information. The associated potential-energy and centrifugal BOB radial functions are then shown in Fig. 6.

It is important to appreciate that the value of the dissociation energy for the $A\,^1\Sigma^+$ state is constrained by the relationship

$$\mathfrak{D}_e(A) = \mathfrak{D}_e(X) + E_{\rm Ag}(5p^2P_{1/2}) - T_e(A), \qquad (12)$$

where $E_{\rm Ag}(5p\,^2P) = 29\,552.05$ cm^{-1} is the accurately known[57] Ag atom electronic excitation energy. As a result, the overall uncertainty in the *A*-state dissociation energy is defined by those for $\mathfrak{D}_e(X)$ and $T_e(A)$, so our estimated overall uncertainty for $\mathfrak{D}_e(A)$ (see Table IV) is essentially the same as that for $\mathfrak{D}_e(X)$. However, for any given value of $\mathfrak{D}_e(X)$, the value of $\mathfrak{D}_e(A)$ must be specified to four decimal places (in spite of its overall ± 200 cm^{-1} uncertainty) in order to yield a value of $T_e(A)$ which will accurately reproduce the experimental data.

VI. DISCUSSION AND CONCLUSIONS

The present analysis has quantitatively confirmed Learner's 1962 assertion, as quoted in the Introduction, that apparent irregularities in the spectrum of the $A\,^1\Sigma^+$ state AgH were merely reflections of the unusual shape of its rotationless potential curve. The implications of this unusual shape are illustrated further in Fig. 7, which shows both our rotationless $J=0$ potential and the centrifugally distorted potentials

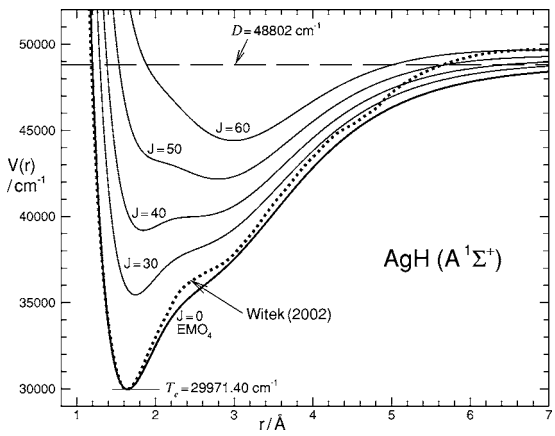

FIG. 7. Illustration of the effect of centrifugal distortion on the the present recommended potential curve for the $A\,^1\Sigma^+$ state AgH (solid curves), and comparison with the rotationless *ab initio* potential of Witek *et al.* (Ref. 25), with the latter shifted to place its minimum at our experimental $T_e(A)$ value.

which define the AgH level energies for selected J values (solid curves). The hydride J range in our data set extends to $J=42$, so the changing shapes seen in Fig. 7 clearly indicate the origin of the unusual band-constant behavior seen in Fig. 4.

Figure 7 also compares the present empirical potential (solid curve) with the best of the *ab initio* potentials reported by Witek *et al.*,[25] after the latter was shifted to our experimental T_e value (see Table IV). In view of the very challenging nature of the *ab initio* calculations, the agreement seen here is remarkably good, and the implausible "ripple" in the theoretical curve near 4.7 Å may well be an artifact due to the fact that their *ab initio* points were represented by a sum of Gaussians.[25]

Our parameter-fit and potential-fit analyses both show that for the ground $X\,^1\Sigma^+$ state BOB effects are modest in magnitude, and that the associated radial functions (see Fig. 6) vary quite slowly with r. For the $A\,^1\Sigma^+$ state, however, those effects are much larger and have a much stronger radial dependence. It is perhaps noteworthy that the distance at which the potential-energy BOB function $\tilde{S}_{\rm ad}^{\rm H}$ begins to drop off sharply is just inside the inner end of the avoided-crossing region where Witek *et al.*[25] showed that the electronic wave function was mainly ionic in character. It is important to realize, however, that the experimental data are only sensitive to these $\tilde{S}_{\rm ad}^{\rm H}$ functions on intervals where data for both AgH and AgD are available (solid curve segments in Fig. 6); in practice, this means between the turning points of the highest observed level of the deuteride. This means that the abrupt reversal in behavior of $\tilde{S}_{\rm ad}^{\rm H}$ for the A state near 1.3 Å is probably merely an extrapolation artifact. In contrast, the experimental data are sensitive to the centrifugal BOB functions $\tilde{R}_{\rm ad}^{\rm H}$ across the entire interval to which they are sensitive to the potential-energy function itself.

The "electronic isotope shift" is defined by the difference between the values of the $\tilde{S}_{\rm ad}^{\rm Ag}(r_e)$ and $\tilde{S}_{\rm ad}^{\rm H}(r_e)$ in the A and X states. Since the available data are unable to determine isotope-dependent well depths for the ground state, this shift (relative to the reference isotopologue ^{107}AgH) is defined as

$$\delta T_e^{(\alpha)}(A) = (\delta M_{\rm Ag}^{(\alpha)}/M_{\rm Ag}^{(\alpha)})u_0^{\rm Ag}(A) + (\delta M_{\rm H}^{(\alpha)}/M_{\rm H}^{(\alpha)})u_0^{\rm H}(A), \tag{13}$$

which yields values of $\delta T_e^{(\alpha)}(A) = -0.0113(\pm 0.0006)$, $-10.487(\pm 0.005)$, and $-10.499(\pm 0.005)$ cm^{-1} for ^{109}AgH, ^{107}AgD, and ^{109}AgD, respectively. Similar estimates of these isotope shifts may be obtained using the $\delta_{0,0}^{\rm Ag}$ and $\delta_{0,0}^{\rm H}$ constants obtained from the parameter-fit analysis.[31] However, they are not expected to be identical because the latter actually define the estimated shift of the hypothetical extrapolated vibrational energy at $v=-1/2$, and do not separate out the higher-order semiclassical corrections associated with Dunham's $Y_{0,0}$ coefficient.[13,58]

ACKNOWLEDGMENT

This research was supported by the Natural Sciences and Engineering Research Council of Canada.

[1] E. Bengtsson and E. Svensson, Compt. Rend. **180**, 274 (1925).
[2] E. Hulthén and R. V. Zumstein, Phys. Rev. **28**, 13 (1926).
[3] E. Bengtsson and E. Olsson, Z. Phys. **72**, 163 (1931).
[4] P. G. Koontz, Phys. Rev. **48**, 138 (1935).
[5] E. Hulthén and E. Knave, *Zeeman, Verhandelingen* (The Hague, The Netherlands, 1935), p. 148.
[6] L. Gerö and R. Schmid, Z. Phys. **121**, 459 (1943).
[7] R. C. M. Learner, Proc. R. Soc. London, Ser. A **269**, 327 (1962).
[8] G. Herzberg, *Spectra of Diatomic Molecules* (Van Nostrand, New York, 1950).
[9] U. Ringström, Ark. Fys. **21**, 145 (1961).
[10] U. Ringström and N. Åslund, Ark. Fys. **32**, 19 (1965).
[11] H. Birk and H. Jones, Chem. Phys. Lett. **161**, 27 (1989).
[12] R.-D. Urban, H. Birk, P. Polomsky, and H. Jones, J. Chem. Phys. **94**, 2523 (1991).
[13] J. L. Dunham, Phys. Rev. **41**, 721 (1932).
[14] J. Y. Seto, Z. Morbi, F. Charron, S. K. Lee, P. F. Bernath, and R. J. Le Roy, J. Chem. Phys. **110**, 11756 (1999).
[15] T. Okabayashi and M. Tanimoto, J. Mol. Spectrosc. **204**, 159 (2000).
[16] J. P. Desclaux and P. Pyykkö, Chem. Phys. Lett. **39**, 300 (1976).
[17] P. Pyykkö, J. Chem. Soc. Faraday Trans. 2 **75**, 1256 (1979).
[18] B. A. Hess and P. Chandra, Phys. Scr. **36**, 414 (1986).
[19] K. Balasubramanian, J. Chem. Phys. **93**, 8061 (1990).
[20] C. L. Collins, K. G. Dyall, and H. F. Schaefer III, J. Chem. Phys. **102**, 2024 (1996).
[21] A. K. Mohanty and F. A. Parpia, Phys. Rev. A **54**, 2863 (1996).
[22] T. Suzumura, T. Nakjima, and K. Hirao, Int. J. Quantum Chem. **75**, 757 (1999).
[23] A. Avramopoulos, V. E. Ingamells, M. G. Papadopoulos, and A. J. Sadlej, J. Chem. Phys. **114**, 198 (2000).
[24] H. A. Witek, T. Nakijima, and K. Hirao, J. Chem. Phys. **113**, 8015 (2000).
[25] H. A. Witek, D. G. Fedorov, K. Hirao, A. Viel, and P.-O. Widmark, J. Chem. Phys. **116**, 8386 (2002).
[26] Y. Li, H.-P. Libermann, R. J. Buenker, and L. Pichl, Chem. Phys. Lett. **389**, 101 (2004).
[27] M. R. Carleer, Proc. SPIE **4168**, 337 (2001).
[28] A. G. Maki and J. S. Wells, *Wavenumber Calibration Tables from Heterodyne Frequency Measurements* (NIST Special Publication 821, U.S. Government Printing Office, Washington, 1991).
[29] B. Edlén, Metrologia **2**, 71 (1966).
[30] W. Whaling, W. H. C. Anderson, M. T. Carle, J. W. Brault, and H. A. Zarem, J. Res. Natl. Inst. Stand. Technol. **107**, 149 (2002).
[31] See EPAPS Document No. E-JCPSA6-123-002538 for ASCII files containing listings of the data used in the present work, the complete parameter set yielded by the global Dunham-type analysis described in Sec. V B, and sets of band constants generated from those Dunham parameters. This document can be reached via a direct link in the online article's HTML reference section or via the EPAPS homepage (http://www.aip.org/pubservs/epaps.html).
[32] R. J. Le Roy, J. Mol. Spectrosc. **194**, 189 (1999).
[33] A.-R. Hashemi-Attar, C. L. Beckel, W. N. Keepin, and S. A. Sonnleitner, J. Chem. Phys. **70**, 3881 (1979); A.-R. Hashemi-Attar and C. L. Beckel, *ibid.* **71**, 4596 (1979); C. L. Beckel and R. B. Kwong, *ibid.* **73**, 4698 (1980); C. L. Beckel, R. B. Kwong, A.-R. Hashemi-Attar, and R. J. Le Roy, *ibid.* **81**, 66 (1984).
[34] R. J. Le Roy and W.-H. Lam, Chem. Phys. Lett. **71**, 544 (1980).
[35] R. J. Le Roy, J. Chem. Phys. **101**, 10217 (1994).
[36] D. R. T. Appadoo, R. J. Le Roy, P. F. Bernath, S. Gerstenkorn, P. Luc, J. Vergès, J. Sinzelle, J. Chevillard, and Y. D'Aignaux, J. Chem. Phys. **104**, 903 (1996).
[37] R. J. Le Roy, DPARFIT 3.3, *A Computer Program for Fitting Multiisotopologue Diatomic Molecule Spectra*, University of Waterloo Chemical Physics Research Report CP-660, 2005. The source code and manual for this program may be obtained from the "Computer Programs" link at http://leroy.uwaterloo.ca
[38] J. G. Ashmore and J. Tellinghuisen, J. Mol. Spectrosc. **119**, 68 (1986).
[39] J. Tellinghuisen, J. Chem. Phys. **118**, 3532 (2003).
[40] J. K. G. Watson, J. Mol. Spectrosc. **80**, 411 (1980).
[41] J. F. Ogilvie, J. Phys. B **27**, 47 (1994).
[42] The notation for BOB correction functions used here differs that of our earlier work (Refs. 32 and 48) in an effort to make it more consistent with that used by others (Refs. 40, 41, and 43) and to avoid confusion with the q notation commonly used for Λ-doubling parameters. Note, however,

that our use of the reference-isotopologue convention of Ref. 32 means that the present $\widetilde{S}^A_{\rm ad}(r)$ differs from Watson's (Refs. 40 and 43) $\widetilde{S}^A(r)$ by the factor $\Delta M_A^{(\alpha)}/m_e$ and that our $\widetilde{R}^A_{\rm na}(r)$ differs from his $\widetilde{R}^A(r)$ by the factor $M_A^{(1)}/m_e$, where m_e is the electron mass.

[43] J. K. G. Watson, J. Mol. Spectrosc. **223**, 39 (2004).

[44] Y. Huang and R. J. Le Roy, J. Chem. Phys. **119**, 7398 (2003).

[45] R. J. Le Roy, J. Y. Seto, and Y. Huang, DPotFit 1.0, *A Computer Program for Fitting Diatomic Molecule Spectra to Potential Energy Functions*, University of Waterloo Chemical Physics Research Report CP-662, 2005; see the "Computer Programs" link at http://leroy.uwaterloo.ca

[46] A. A. Šurkus, R. J. Rakauskas, and A. B. Bolotin, Chem. Phys. Lett. **105**, 291 (1984).

[47] Y. Huang, M.Sc. thesis, Department of Chemistry, University of Waterloo, 2001.

[48] R. J. Le Roy and Y. Huang, J. Mol. Struct.: THEOCHEM **591**, 175 (2002).

[49] R. J. Le Roy, LEVEL 7.7, *A Computer Program for Solving the Radial Schrödinger Equation for Bound and Quasibound Levels*, University of Waterloo Chemical Physics Research Report CP-661, 2005; see the "Computer Programs" link at http://leroy.uwaterloo.ca

[50] K. P. Huber and G. Herzberg, *Constants of Diatomic Molecules* (Van Nostrand Reinhold, New York, 1979).

[51] A. Kant and K. A. Moon, High. Temp. Sci. **11**, 52 (1979).

[52] R. J. Le Roy, J. Mol. Spectrosc. **191**, 223 (1998).

[53] Subroutine NLLSSRR for performing linear or nonlinear least-squares fits and automatically performing the sequential rounding and refitting discussed in Ref. 52 may be downloaded freely via the "computer programs" link on the www site http://leroy.uwaterloo.ca

[54] R. Rydberg, Z. Phys. **73**, 376 (1931); O. Klein, *ibid.* **76**, 226 (1932); R. Rydberg, *ibid.* **80**, 514 (1933); A. L. G. Rees, Proc. Phys. Soc. London **59**, 998 (1947).

[55] R. J. Le Roy, RKR1 2.0, *A Computer Program Implementing the First-Order RKR Method for Determining Diatomic Molecule Potential-Energy Curves*, University of Waterloo Chemical Physics Research Report CP-657, 2003. The source code and manual for this program may be obtained from the "Computer Programs" link at http://leroy.uwaterloo.ca

[56] J. M. Hutson, J. Phys. B **14**, 851 (1981); J. M. Hutson, QCPE Bulletin, 2, No. 2, Program #435, Quantum Chemistry Program Exchange, Indiana University, Bloomington, Indiana.

[57] C. E. Moore, *Atomic Energy Levels as Derived from the Analyses of Optical Spectra* (National Bureau of Standards, Washington, DC, 1958), Vol. 3.

[58] A. Adohi-Krou, F. Martin, A. J. Ross, C. Linton, and R. J. Le Roy, J. Chem. Phys. **121**, 6309 (2004).